The Astrophysical Journal, 700:L182–L186, 2009 August 1 doi:10.1088/0004-637X/700/2/L182

"EXTREME ULTRAVIOLET WAVES" ARE WAVES: FIRST QUADRATURE OBSERVATIONS OF AN EXTREME ULTRAVIOLET WAVE FROM *STEREO*

Spiros Patsourakos[1] and Angelos Vourlidas[2]
[1] George Mason University, Fairfax, VA 22030, USA; spiros.patsourakos@nrl.navy.mil
[2] Code 7663, Naval Research Laboratory, Washington, DC 20375, USA; vourlidas@nrl.navy.mil
Received 2009 May 13; accepted 2009 June 3; published 2009 July 20

ABSTRACT

The nature of coronal mass ejection (CME)-associated low corona propagating disturbances, "extreme ultraviolet (EUV) waves," has been controversial since their discovery by EIT on *SOHO*. The low-cadence, single-viewpoint EUV images and the lack of simultaneous inner corona white-light observations have hindered the resolution of the debate on whether they are true waves or just projections of the expanding CME. The operation of the twin EUV imagers and inner corona coronagraphs aboard *STEREO* has improved the situation dramatically. During early 2009, the *STEREO* Ahead (STA) and Behind (STB) spacecrafts observed the Sun in quadrature having a ≈90° angular separation. An EUV wave and CME erupted from active region 11012, on February 13, when the region was exactly at the limb for STA and hence at disk center for STB. The *STEREO* observations capture the development of a CME and its accompanying EUV wave not only with high cadence but also in quadrature. The resulting unprecedented data set allowed us to separate the CME structures from the EUV wave signatures and to determine without doubt the true nature of the wave. It is a fast-mode MHD wave after all.

Key words: Sun: coronal mass ejections (CMEs)

Online-only material: mpeg animations

1. INTRODUCTION

An important discovery of *SOHO*/EIT (Delaboudinière et al. 1995) was the detection of large-scale extreme ultraviolet (EUV) disturbances traveling over significant fractions of the solar disk (e.g., Moses et al. 1997; Thompson et al. 1998, 1999). EUV waves emanate from flaring active regions (ARs) but are strongly associated with coronal mass ejection (CME) onsets (e.g., Biesecker et al. 2002; Patsourakos et al. 2009). Despite the observations of hundreds of EUV waves over a full solar cycle, their origin is still strongly debated. A rather obvious mechanism is a fast-mode MHD wave triggered by the eruption (e.g., Thompson et al. 1999; Wang 2000; Wu et al. 2001; Ofman & Thompson 2002; Vršnak et al. 2002; Warmuth 2007; Linker et al. 2008). This interpretation accounts for their association with Hα Moreton waves, their low average speeds (a few hundred km s^{-1}; Long et al. 2008; Veronig et al. 2008; Gopalswamy et al. 2009 for the latest *STEREO* results), and is the expected plasma behavior after a sudden energy release (e.g., a flare and/or CME). However, expanding EUV dimmings are often observed at the wake of EUV waves and sometimes develop "stationary" fronts which could, in principle, pose problems to a wave interpretation. Several authors have thus suggested that EIT waves are the footprints or the low coronal extensions of the associated CMEs, and thus are "pseudo-waves" (e.g., Delannée 2000; Chen et al. 2002; Attrill et al. 2007; Delannée et al. 2008). See also the review by Warmuth (2007) and Patsourakos et al. (2009) for a compilation of *STEREO* observational tests for the various wave theories and their comparison with actual *STEREO* observations.

The main reason for the lingering controversy is the lack of observations with appropriate cadence, and field-of-view (FOV) coverage to allow separation between the various facets of the CME and of the wave. EUV waves are better observed when their source region is close to disk center, which allows monitoring their propagation over large areas of the solar disk. On the other hand, CMEs are better observed off-limb or close to limb, which allows us to track their low-coronal radial and lateral evolution. Clearly, the single-viewpoint *SOHO* observations could address either the wave or the CME onset but never *both* of them at the *same* time. Significant confusion on the nature of the propagating features associated with the EUV waves has also been caused by the relatively low cadence (≈12 minutes) of the EIT observations. Finally, the lack of an inner white light coronagraph (WLC) on *SOHO* hindered comparisons of simultaneous EUV images of waves and WLC images of the associated CMEs.

Obviously, the optimal observing configuration for solving the EUV wave problem is simultaneous EUV-coronagraph observations in *quadrature*. This was not possible until the launch of the *STEREO* mission in late 2006 (Kaiser et al. 2008). By early 2009, the two spacecrafts reached a separation of ≈90°, ideal for EUV wave observations.

Here we present the first quadrature observations of an EUV wave. It emanated from an AR at disk center as viewed from *STEREO* Behind (STB), but located at the limb as viewed from *STEREO* Ahead (STA). Moreover, we have EUV images at a higher cadence than the *SOHO* ones and WLC coverage of the inner corona (Section 2). With this unique data set, we were able to simultaneously follow the early evolution of the EUV wave and the CME at quadrature (Section 2.1). It was rather straightforward to determine that the EUV wave is indeed a real MHD wave and not a pseudo-wave (Sections 2.2 and 2.3).

2. OVERVIEW OF THE CME–WAVE OBSERVATIONS

We use EUV and total brightness (TB) WLC images from the Extreme Ultraviolet Imaging Telescope (EUVI; Wuelser et al. 2004) and the COR1 coronagraph (Thompson et al. 2003), respectively, of the Sun–Earth Connection Coronal and Heliospheric Investigation (SECCHI; Howard et al. 2008) instrument suite. EUVI observes the entire solar disk and the

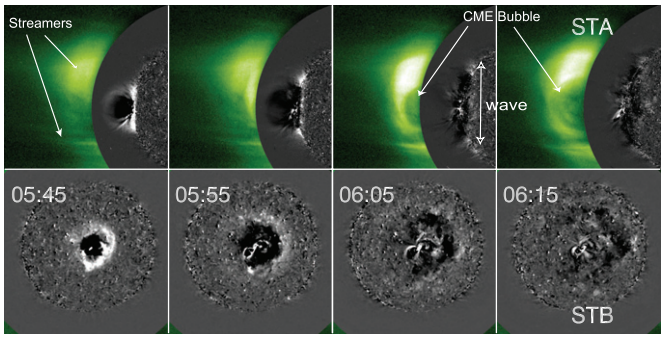

Figure 1. Overview of the quadrature observations of an EUV wave. Composite EUVI 195 RD images (grayscale; black (white) implies intensity decrease (increase), respectively) and COR1 TB images (intensity increases with color from black–white–green): upper row STA; lower row STB. The images for a given instrument were obtained simultaneously on the Sun but the time tags correspond to times for STA.

(An mpeg animation of this figure is available in the online journal.)

corona up to 1.4 $R_{\odot}$. We use images from the 171 and 195 Å (hereafter 171 and 195) channels and our EUVI observations have a cadence of 2.5 minutes (5 in STB) in 171 and 10 minutes in 195. The COR1 coronagraph observes the corona in 1.5–4 $R_{\odot}$ with a 10 minute cadence.

The event took place on 2009 February 13 during a period of deep solar minimum dominated by quiet Sun. Only a single small active region 11012 was present over 270° of solar longitude. This unusually "clean" background helped to unambiguously track various features associated with the observed wave event at large distances. A flare–"EUV wave"–CME event originated from this region, starting at ≈05:35. The flare was weak (GOES B2.3) and the corresponding CME was slow (≈350 km s^{-1} as determined by *CaCTus*; Robbrecht & Berghmans 2004).

Video1.mpg in the online journal contains STA and STB 195 plain images. Snapshots from the event in 195 and COR1 are shown in Figure 1 and the full development of the wave and the CME can be seen in video2.mpg in the online journal. The 195 images are running difference (RD) images (i.e., from each image we subtract the one 10 minutes earlier). The COR1 images are TB images. FESTIVAL software (Auchère et al. 2008) was used to generate the composite EUVI–COR1 images. COR1-B images are not shown here because they do not provide useful information. The CME is a halo in COR1-B and is only faintly visible late (after 06:55). Starting at 05:35, we observe in EUVI-A a bubble developing both radially and laterally. The bubble is bounded by streamers in both the north and south. When it emerges in the COR1-A FOV at 05:55, it becomes a rather typical three-part structure CME. At the same time, the CME pushes aside streamers on either side. The southern streamer deflection is especially obvious in Figure 1. Note that the CME cavity in COR1-A and the EUVI bubble are clearly the same structure (frames at 05:55–06:25). However, the white-light signature of the CME is much larger than its EUVI counterpart, mostly toward the north. The COR1-A CME flanks map very accurately to EUVI dimmings on either side of the AR and are due to loops deflected by the EUV wave. By 05:45, the latitudinal extent of the wave becomes larger than the CME extent. Hence, the STA data alone reveal very clearly that the CME and the EUV wave are distinct structures (as also speculated in the review by Harrison 2009 which was based on pre-*STEREO* data) with different spatial scales but they also show that the wave-induced deflections contribute to the width of the white light CME. It is the later contribution that complicates any CME–wave study that lacks the data coverage of Figure 1.

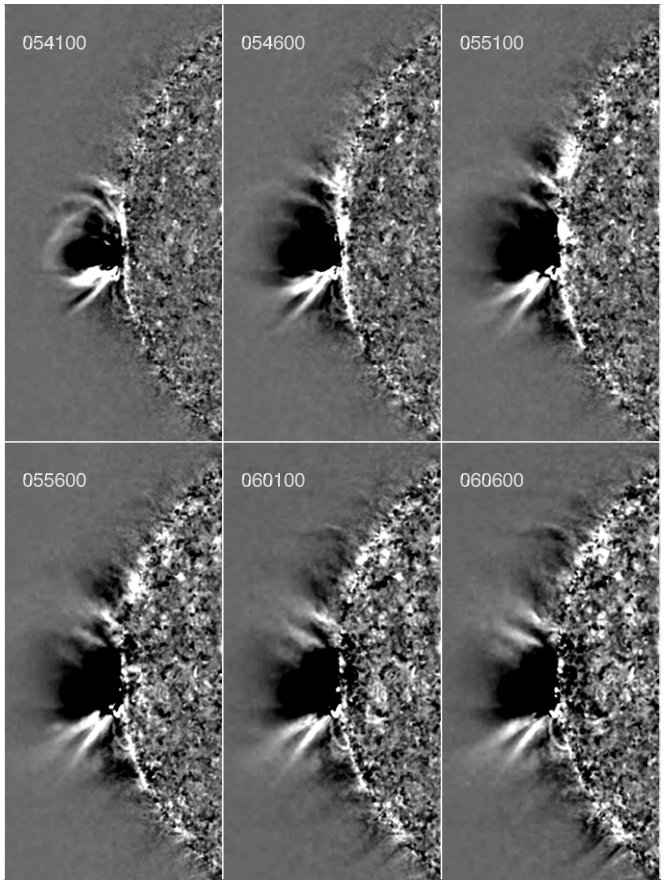

Figure 2. Sample snapshots from the 171 SC A image sequence in 10 minutes running difference format. Black (white) corresponds to intensity decrease (increase).

(An mpeg animation of this figure is available in the online journal.)

In EUVI-B, we observe a set of loops that erupt before the wave forms, which could be a typical pattern in wave formation (e.g., Patsourakos et al. 2009). The wave exhibits quasi-circular expansion over most of the visible disk, which is a typical feature of solar minimum EUV waves (e.g., Moses et al. 1997; Thompson et al. 1998). There is very little wave expansion toward the southeast because of the existence of a coronal hole on the eastern side of the AR. The wave becomes more diffuse as it propagates away from the region and disappears when it reaches the western limb of EUVI-B, around 06:15. In EUVI-A, the wave extends to about the central meridian. The latitudinal extension of the wave is the same in both EUVI-A and B.

2.1. High-Cadence CME–Wave Observations

The high cadence (2.5 minutes) of the EUVI 171 data allowed us to understand the nature of the propagating features associated with the EUV wave. We used a 171 EUVI-A movie (video3.mpg in the online journal) of wavelet contrast–enhanced images (Stenborg et al. 2008). Sample 10 minute RD frames are given in Figure 2.

As we saw in the 195 images, a set of low-lying loops, in the shape of a bubble, starts to slowly rise at ≈05:28. By 05:41, we see the formation of a dimming at the center of the AR and the first indications of loop deflections on either side of the expanding bubble. The deflections appear

as black–white pairs in the RD images and propagate away from the expanding bubble along the north–south direction. They induce transverse oscillations in coronal structures at the solar limb. The oscillations damp within 10 minutes and their maximum amplitude decreases with distance from the source. The outermost deflected structures seem to match with the latitudinal extent of the wave as seen on the disk strongly suggesting their association. These deflections are likely the off-limb counterpart of the transverse (kink-like) oscillations seen in AR loops in the wake of an eruption (e.g., Aschwanden et al. 1999; Nakariakov et al. 1999; Verwichte et al. 2005). The observed off-limb EUV deflections are not uncommon: they have been observed in EUVI high-cadence movies of eruptions at the limb. Similar deflection phenomena have been observed with coronagraph in association with CMEs (e.g., Gosling et al. 1974; Sheeley et al. 2000; Vourlidas et al. 2003; Liu et al. 2009). The present event showed also evidence of a streamer deflection in the coronagraph data (e.g., Figure 1). The deflections can only be explained by the passage of a wave and are therefore a very strong indication that the EUV wave is indeed a wave. MHD simulations show ample evidence for deflected coronal structures once a velocity pulse (i.e., an eruption) is set up (e.g., Vourlidas et al. 2003; Ofman 2009 for a review).

2.2. CME–Wave Kinematics

To clarify further the difference in the nature of the CME and the EUV wave, we performed *simultaneous* measurements of the CME and wave widths. In determining the wave width, we followed the method of Podladchikova & Berghmans (2005). We used 195 and 171 STB BD images where we subtracted a pre-event reference image taken at 05:00. All images were differentially rotated to the time of the reference image. The BD images were first projected onto a spherical polar coordinate system (ϕ–r) with its center on the eruption site. Data were then discretized on a grid with a $d\phi = 45^\circ$ and $dr = 0.075\ R_\odot$ (or 50 Mm). We averaged those maps over the sectors in the northwest direction, where the wave was best visible (Figure 1) and obtained radial intensity-ratio profiles. The wave front location corresponds to the local maxima of these curves. The wave width error bar was set to dr.

For the determination of the CME width, we used the wavelet contrast–enhanced 171 EUVI-A images of the CME bubble. The latter was defined as the outermost set of loops which were "opened" by the eruption and remained opened. They correspond to the "deep" dimming seen in the AR core after the eruption (i.e., the dark central area of Figure 2). No deflections were seen within this area which is consistent with an ejection and not the passage of a wave. The EUV bubble can be further traced to the COR1 FOV (e.g., the three leftmost panels of Figure 1) and was visible in 171 between ≈05:36 and 05:56. We manually selected a series of points outlining the bubble and fit them with a circle. The radius of the best-fit circle supplied the width of the CME bubble. We estimated error bars using the standard deviation of the residuals between the best-fit circle radius and the distances of the manually selected points using the best-fit circle center as a reference. The above process was also applied to COR1 A images of the CME bubble from 06:10 to 06:35.

The CME–wave width measurements are in Figure 3. First note that the 171 and 195 wave measurements are consistent with each other. Quadratic fits to the wave width give a linear expansion speed of ≈250 km s^{-1} and a deceleration of ≈−25 m s^{-2}, typical values for EUV waves. The evolution

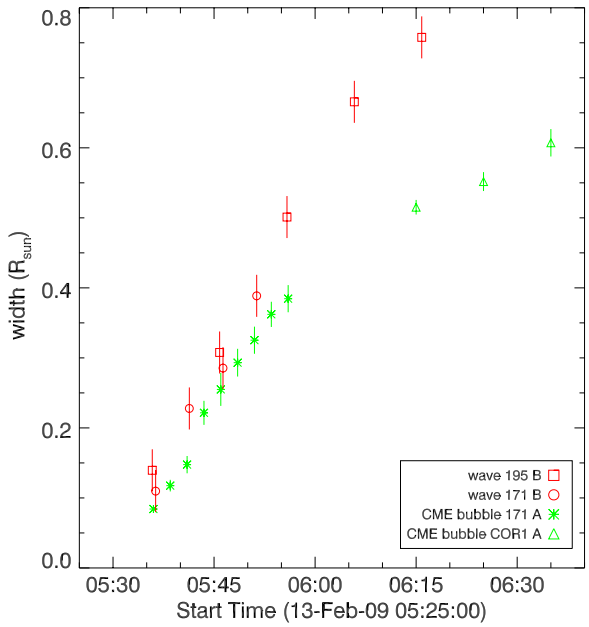

Figure 3. Time evolution of the CME–wave widths from STA and STB, respectively. See Section 2.2.

of the CME width exhibited two phases: first, a period of strong lateral expansion in the EUVI FOV, followed by a slower expansion in the COR1 FOV. The important result in Figure 3 is that while the CME–wave widths track each other quite closely in the beginning of the event, the wave becomes significantly wider that the CME after ≈05:45. This is in disagreement with the predictions of pseudo-wave theories which require that the projected CME width or its low coronal extension to match the wave width at all times.

2.3. Three-dimensional CME–Wave Modeling

Finally, we performed forward modeling of the observed CME and wave using the simplest instance of the three-dimensional forward model of Thernisien et al. (2006, 2009): a spherical bubble attached to a conical leg. The free parameters of the model were varied until we found a satisfactory projection of the model into the STA sky plane (see Patsourakos et al. 2009 for details on the application of this model to EUVI and COR1 data). The geometrical modeling is helpful in identifying the differences between the CME and the EUV wave, as discussed below. However, a full three-dimensional MHD study is needed for more complete modeling of the physical phenomena seen in this observation.

Figure 4 shows the CME–wave modeling for the observations at 06:05. We selected this time because the wave has covered a significant part of the visible disk in STB (panel a) while part of the CME bubble has entered into the COR1-A FOV (panel b). The model of the CME bubble (panel d; green wireframe) fits the white-light/EUV cavity rather well with the exception of the rapidly converging legs of the cavity. This is a limitation of our geometric model. A larger model was then used to fit the outer boundary of the coronal volume affected by the eruption (panel d; red wireframe). The model encompasses the latitudinal extent of the EUV wave in STA (compare with panel b) which is comparable to the latitudinal extension of the off-limb deflected structures (Section 2.3). We note though that the model somehow overestimates the southward extension of the off-limb volume affected by the wave. Panel (c) contains the disk

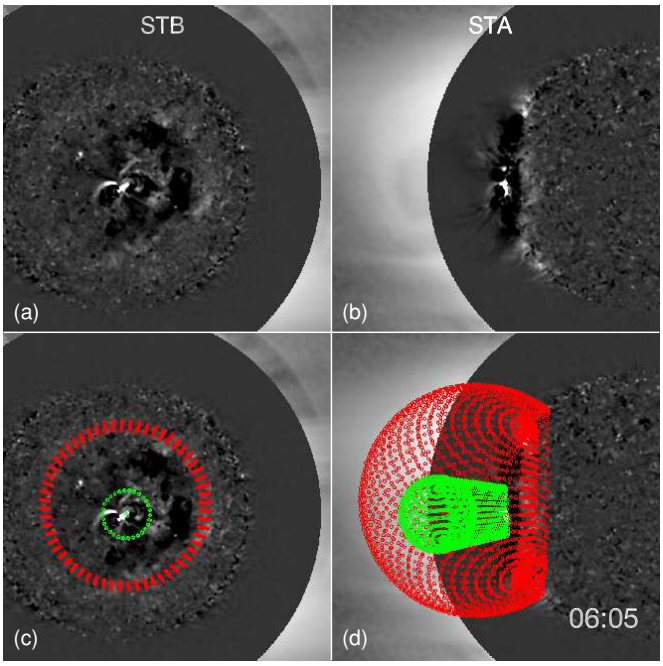

Figure 4. Forward modeling of the CME and wave three-dimensional shape in both *STEREO* spacecrafts for observations at 06:05. Panels (a) and (b) contain composite EUVI 195 RD and COR1 TB images from STB and STA. Panel (d) contains the best-fit CME (green wireframe) and wave (red wireframe) model determined for STA. Panel (c) has the disk projections of these models in STB.

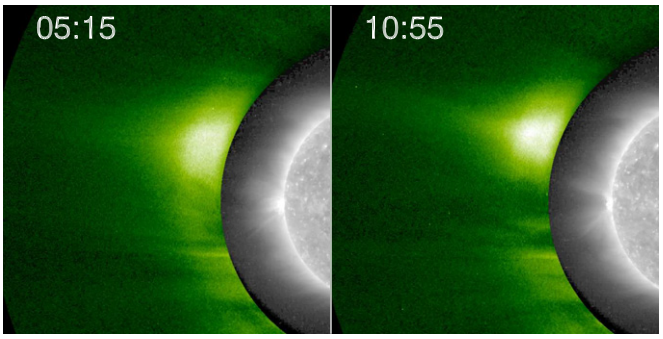

Figure 5. Composite of plain 195 and TB COR1 STA images before and after the event (left and right panels, respectively).

projections (in STB) of the models. The wave projection fits rather well the extent of the wave, while the CME projection is smaller and confined around the deep AR core dimming. The forward modeling suggests that the wave and the CME are not concentric with each other or with the AR center. The wave offset is likely due to the influence of the coronal hole at the east of the erupting AR. The CME offset is caused by the westward location of the erupted loops in the AR core.

Therefore, the three-dimensional modeling reveals the different scales and nature of the CME and the wave and provides a straightforward explanation for the white light extension of the event which is commonly referred to as the "white light CME." It is the latter, rather careless, use of terminology that seems to be the cause of confusion in EUV wave studies.

3. CONCLUSIONS

As discussed in Section 1, the exact nature of the EUV waves (MHD waves or pseudo-waves) and their association with CME structures have been the matter of intense debate since their discovery. The main reason was the lack of high-cadence comprehensive coverage of the early development of the wave and of the associated CME.

A second reason is the careless use of the term "CME" in a generic way to variously describe the ejected fluxrope, the full extent of the white light brightness enhancements and the extent of EUV dimmings in the low corona. Our observations demonstrate that the EUV wave and the CME are initially connected and later become separate phenomena.

We use the unique SECCHI observations presented above to clarify both the nature of EUV waves and the CME terminology. For the latter, we reserve the term "CME" only for the actual ejected coronal magnetic structure: the fluxrope from the AR core. This is further illustrated in Figure 5, where it is clear that only the AR core loops and overlying corona have been removed by the CME, whereas a much larger coronal volume, including the adjacent streamers, that participated in the event (or was affected by it) stayed put after the eruption. This work shows clearly that our proper definition leads to a better understanding of the CME and its effects on the surrounding corona.

The high-cadence, quadrature SECCHI observations of a typical EUV wave/CME event led us to significantly new insights on the nature and development of EUV waves and CMEs. Our main findings are as follows.

1. The CME is born from the transformation of a set of rising loops in the core of the AR to a rapidly expanding EUV bubble/cavity.
2. The impulsive acceleration of the CME bubble induces deflections on progressively remote coronal structures which match with the latitudinal extent of the wave.
3. The expanding CME evacuates a significant part of the AR corona leading to stationary dimmings on the scale of the AR.
4. The expanding EUV wave is tracked by a diffuse weak intensity enhancement with a trailing dimming disturbance in the low corona and by deflections of distant (from the AR) streamers higher in the corona.
5. After a few minutes (≈15 minutes), the wave width becomes significantly larger than the CME one. The CME width is determined by the expanding cavity.
6. Three-dimensional geometrical modeling of the CME and wave structures shows unambiguously that they correspond to different structures: the wave occupies and affects a much bigger volume than the CME.

All of the above findings are consistent only with an expanding fast-mode wave from the site of an impulsive energy release. They are also consistent with a driven wave (by an expanding CME) and not with a blast wave (induced by a flare). These findings, especially the distant streamer and EUV off-limb structures deflections, are inconsistent with the notion that EUV waves are pseudo-waves, i.e., the disk projection or the lower coronal extent of the CME. We must conclude, therefore, that the observed wave is a true MHD wave, as demonstrated by past MHD models (e.g., Wu et al. 2001; Ofman & Thompson 2002; Ofman 2007; Linker et al. 2008). The wave is driven by the expanding CME. The propagating deflections seen in the off-limb coronal structures and in the white light streamers higher up serve as a "smoking-gun" of the passage of a wave in the corona.

We emphasize here that our discussion applies only to propagating disturbances reaching global scales. Such events are typical of solar minimum conditions, when few ARs are

present, and most of the solar disk is occupied by quiet Sun. The expanding CME cavity and stationary dimmings in the AR could very well be accounted for by the pseudo-wave theories (e.g., Zhukov & Auchère 2004). It could be well that the observed wave, in the period before wave and CME start to decouple (i.e., 05:45), was indeed a pseudo-wave.

There are also occasions, particularly under solar maximum conditions when multiple ARs are present, where EUV dimmings develop away from the AR and after the wave has passed from these areas. Those dimmings could originate from reconnections with the expanding CME fluxrope. So there is no reason to discard those theories at the moment. Only their application needs to be carefully considered. Our observations and analysis demonstrate the separation between the CME eruption and the EUV wave propagation.

The SECCHI data used here were produced by an international consortium of the Naval Research Laboratory (USA), Lockheed Martin Solar and Astrophysics Lab (USA), NASA Goddard Space Flight Center (USA), Rutherford Appleton Laboratory (UK), University of Birmingham (UK), Max-Planck-Institut for Solar System Research (Germany), Centre Spatiale de Liège (Belgium), Institut d Optique Théorique et Appliqueé (France), and Institut d'Astrophysique Spatiale (France). We thank G. Stenborg for supplying wavelet images and B. Kliem, V. Ontiveros, and the referee for useful comments.

REFERENCES

Aschwanden, M. J., Fletcher, L., Schrijver, C. J., & Alexander, D. 1999, ApJ, 520, 880
Attrill, G. D. R., Harra, L. K., van Driel-Gesztelyi, L., & Démoulin, P. 2007, ApJ, 656, L101
Auchère, F., Soubrié, E., Bocchialini, K., & Legall, F. 2008, Sol. Phys., 248, 213
Biesecker, D. A., Myers, D. C., Thompson, B. J., Hammer, D. M., & Vourlidas, A. 2002, ApJ, 569, 1009
Chen, P. F., Wu, S. T., Shibata, K., & Fang, C. 2002, ApJ, 572, L99
Delaboudinière, J.-P., et al. 1995, Sol. Phys., 162, 291
Delannée, C. 2000, ApJ, 545, 512
Delannée, C., Török, T., Aulanier, G., & Hochedez, J.-F. 2008, Sol. Phys., 247, 123
Gopalswamy, N., et al. 2009, ApJ, 691, L123
Gosling, J. T., Hildner, E., MacQueen, R. M., Munro, R. H., Poland, A. I., & Ross, C. L. 1974, J. Geophys. Res., 79, 4581
Harrison, R. 2009, in Proc. IAU Symp. 257, Universal Heliophysical Processes, ed. N. Gopalswamy & D. F. Webb (Cambridge: Cambridge Univ. Press), 191
Howard, R., et al. 2008, Space Sci. Rev., 136, 67
Kaiser, M. L., et al. 2008, Space Sci. Rev., 136, 5
Linker, J. A., Lionello, R., Mikic, Z., Titov, V., & Riley, P. 2008, AGU Spring Meeting Abstracts, 5
Liu, Y., Luhmann, J. G., Bale, S. D., & Lin, R. P. 2009, ApJ, 691, L151
Long, D. M., Gallagher, P. T., McAteer, R. T. J., & Bloomfield, D. S. 2008, ApJ, 680, L81
Moses, D., et al. 1997, Sol. Phys., 175, 571
Nakariakov, V. M., Ofman, L., Deluca, E. E., Roberts, B., & Davila, J. M. 1999, Science, 285, 862
Ofman, L. 2007, ApJ, 655, 1134
Ofman, L. 2009, Space Sci. Rev. (http://www.springerlink.com/content/jr56225283mqn575/?p=2a26a99cb7d04cb7acod1cffbc8a47fa&pi=9)
Ofman, L., & Thompson, B. J. 2002, ApJ, 574, 440
Patsourakos, S., Vourlidas, A., Wang, Y.-M., Stenborg, G., & Thernisien, A. 2009, arXiv:0905.2189
Podladchikova, O., & Berghmans, D. 2005, Sol. Phys., 228, 265
Robbrecht, E., & Berghmans, D. 2004, A&A, 425, 1097
Sheeley, N. R., Hakala, W. N., & Wang, Y.-M. 2000, J. Geophys. Res., 105, 5081
Stenborg, G., Vourlidas, A., & Howard, R. A. 2008, ApJ, 674, 1201
Thernisien, A. F. R., Howard, R. A., & Vourlidas, A. 2006, ApJ, 652, 763
Thernisien, A. F., Vourlidas, A., & Howard, R. 2009, Sol. Phys., 256, 111
Thompson, B. J., Plunkett, S. P., Gurman, J. B., Newark, J. S., St. Cyr, O. C., & Michels, D. J. 1998, Geophys. Res. Letters, 25, 2465
Thompson, B. J., et al. 1999, ApJ, 517, L151
Thompson, W. T., et al. 2003, Proc. SPIE, 4853, 1
Veronig, A. M., Temmer, M., & Vršnak, B. 2008, ApJ, 681, L113
Verwichte, E., Nakariakov, V. M., & Cooper, F. C. 2005, A&A, 430, L65
Vourlidas, A., Wu, S. T., Wang, A. H., Subramanian, P., & Howard, R. A. 2003, ApJ, 598, 1392
Vršnak, B., Warmuth, A., Brajša, R., & Hanslmeier, A. 2002, A&A, 394, 299
Wang, Y.-M. 2000, ApJ, 543, L89
Warmuth, A. 2007, Lecture Notes in Physics 725, The High Energy Solar Corona: Waves, Eruptions, Particles (Heidelberg: Springer), 107
Wu, S. T., Zheng, H., Wang, S., Thompson, B. J., Plunkett, S. P., Zhao, X. P., & Dryer, M. 2001, J. Geophys. Res., 106, 25089
Wuelser, J. P., et al. 2004, Proc. SPIE, 5171, 111
Zhukov, A. N., & Auchère, F. 2004, A&A, 427, 705